Article

Preparation of a New Adsorbent Material from Agro-Industrial Waste and Comparison with Commercial Adsorbent for Emerging Contaminant Removal

Luís Fernando Cusioli [1,*], Daniel Mantovani [1], Rosângela Bergamasco [2], Angelo Marcelo Tusset [1] and Giane Gonçalves Lenzi [1]

1   Post-Graduate Program in Production Engineering (PPGEP), Federal University of Technology (UTFPR), Ponta Grossa 84017-220, Paraná, Brazil
2   Department of Chemical Engineering, State University of Maringá, Maringá 87020-900, Paraná, Brazil
*   Correspondence: luiscusioli@gmail.com

Abstract: An adsorbent was developed from agro-industrial residues derived from the seed husks of *Moringa oleifera* Lam., in which the hydrochar process was used as it is a sustainable, low-cost and easy-to-operate process. In comparison, a commercial adsorbent, activated charcoal from babaçu coconut, was used. Both materials were characterized using SEM, FTIR, zeta potential and BET, showing their morphologies, chemical compositions and textural analyses that proved the adsorption capacity of each material. A cost study was also carried out regarding the production of the materials. For both materials, an equilibrium study was carried out using the following contaminants: metformin, diuron, methylene blue and lead. We aimed to study the use of agro-industrial waste as a new adsorbent material, which was shown to have an average removal for all the contaminants tested of around 84.56–99.13%. The new adsorbent developed had many interactions with the studied contaminants, allowing its use on a large scale since its production cost was low. The main objective of this study was thus to compare a commercial activated charcoal with a biosorbent from agro-industrial waste, prepared by the hydrochar method.

Keywords: sustainable material; emerging contaminants; production cost; product quality

1. Introduction

In recent years, the presence of micropollutants in water has become a major concern worldwide. These pollutants, also known as emerging contaminants, are composed of a wide variety of substances of both natural and anthropogenic origin. This category encompasses a variety of substances, such as pharmaceuticals, pesticides, dyes, industrial chemicals and heavy metals, among others [1–4]. These micropollutants are usually found in low concentrations in water resources, ranging from ng L^{-1} to µg L^{-1}. The low concentration and diversity of the compounds present in water not only make detection and analysis procedures more complicated, but also make water treatment processes used for supply and wastewater treatment more difficult [5–7].

Pesticides, widely used in modern agriculture, are considered one of the main sources of environmental pollution due to the high amount of hazardous chemicals that are released into the atmosphere, soil and water [8,9]. While these chemicals are used to increase productivity and profits in the agricultural sector, they have a significant negative impact on human health and biodiversity. Herbicides, fungicides and insecticides are the main types of pesticides that are in use, and their toxicity varies widely depending on the formulation, dose and exposure time [10].

Diuron (3-(3,4-dichlorophenyl)-1,1-dimethylurea) is a substance widely used as an algaecide and herbicide in the arylurea class, whose main effect is the inhibition of photosynthesis [11–13]. It is one of the most common and widespread herbicides in Brazil and,

possibly, worldwide. Among the crops to which it is applied in the country, sugarcane and corn stand out [14,15].

Chemicals known as pharmaceuticals are used for diagnostic, therapeutic, preventive or disease-modifying purposes. This definition also encompasses veterinary pharmaceuticals and illicit drugs [16,17]. A wide range of medicines for humans, such as antibiotics, synthetic hormones, anti-inflammatories, statins and cytotoxins, are produced and consumed, with some examples reaching annual production in the order of thousands of tons [18,19]. When drugs reach the environment, they become a big problem, as their accumulation causes serious damage [20].

The use of dyes in various industries, such as textiles, plastics and paper, generates large volumes of colored effluents that have a direct impact on the environment, especially when disposed of without proper treatment [21,22]. Methylene blue is an example of a cationic dye commonly used in the dyeing of cotton, wool and silk, which can have negative effects on human health and water quality. In addition to reducing sunlight infiltration and affecting photosynthetic activity, dye ingestion can cause symptoms such as burning, vomiting, diarrhea and gastritis [23,24]. It is essential for the industry to adopt sustainable and responsible practices and to carry out proper treatment of these effluents to minimize environmental impacts and protect public health [25].

Heavy metals are pollutants that are not biodegradable and accumulate in groundwater and on the surface of the soil as residues from some industrial processes, such as mining, painting and anti-corrosion coating [26]. Among them, lead (Pb(II)) is considered one of the most toxic heavy metals due to its negative effects on the nervous system, blood circulation, kidneys and human reproductive system [27,28]. Anthropogenic sources of lead contamination include used batteries, lead smelting, tetraethyl lead industries, mining, plating and the glass-ceramic industry. The excessive presence of Pb(II) in fresh water poses a health risk and can contribute to serious diseases such as encephalopathy and hepatitis [29,30].

These emerging contaminants have a high leaching potential, and these contaminants are, for example, capable of contaminating groundwater and surface water. The presence of traces of this substance is observed in several countries, such as Brazil, the United States, China and Germany, among others [31].

When emerging pollutants reach surface- and groundwater, there is a great risk of contamination, which may pose a threat to the health of the population that consumes these waters. Unfortunately, conventional water treatment is often not sufficient to remove these contaminants, which has led to the development of more efficient alternative methods [32,33]. Adsorption has proved to be a highly effective and reliable technique to remove organic pesticides, and is based on the accumulation of substances on the surface of a solid adsorbent. Among the advantages of using this method are their universal natures, low cost and ease of operation [34].

Biosorption is a process that involves the use of biological materials to remove pollutants from the environment, and has been the subject of numerous studies in the environmental area [35]. This is due to the interest in identifying effective and low-cost bio-sorbents for removing pollutants. Agricultural residues are an attractive option for this purpose, as they are rich in lignin and cellulose, which have many functional groups that favor biosorption. In this context, the bark of *Moringa oleifera* Lam. has been considered a promising adsorbent to remove pollutants from the environment [36].

Moringa oleifera Lam., originally from India, is a medium-sized plant that grows in almost all types of soil, with greater development in tropical plains. Its seeds have been widely used as a coagulant in the treatment of water for human consumption [37]. In addition, previous studies have already shown that the bark of the plant has a high potential for removing pollutants in aqueous samples, such as metals and organic compounds [38,39].

As these structures are located inside the adsorbent, their research and development is limited by current experimental methods, which provide little information on the characteristics of the activated carbon component. Therefore, current research is oriented towards

the use of various analysis methods (mainly computational and physical–scientific or chemical). Activated carbon is a porous carbonaceous material with continually expanding applications in water treatment and desalination, wastewater treatment and air purification due to its unique characteristics [40].

Activated carbon is a very diverse adsorbent material, including a high degree of porosity and a high surface area, while up to 90% of it can be constituted by carbon. In addition, the carbon structures contain the main functional groups responsible for the ad-sorption of contaminants [41].

In recent years, there has been a growing interest in research on the use of biomass as a precursor material and on conversion methods to produce useful materials. One of the biomass conversion technologies is hydrothermal carbonization, which is a thermo-chemical process used to produce hydrochar and other materials with high added value [42–44]. Hydrochar is a carbonaceous material obtained from biomass subjected to hydrothermal carbonization, which occurs through the reaction between the precur-sor material and water in an autoclave, with temperatures between 150 and 260 °C and self-generated pressures. The final product can be applied in several areas, including agri-culture, due to its chemical and structural properties that favor the filtration and retention of nutrients, the reduction in leaching and carbon fixation [45].

The objective of this work was to evaluate the adsorption capacity of the husks of *Moringa oleifera* Lam. prepared by the hydrochar method, in comparison with commercial activated carbon, for the removal of emerging pollutants present in contaminated waters, in addition to verifying the costs associated with this technology.

2. Materials and Methods

The experiments were carried out at the Environmental Management, Control and Preservation Laboratory at the Department of Chemical Engineering at the State University of Maringá. The activated carbon used for comparison was donated by a company that operates in the segment based in the city of Maringá in Paraná, Brazil.

2.1. Chemicals

To carry out the work, the following reagents were used: metformin with purity of 99% (Sigma-Aldrich®, Burlington, MA, USA), diuron with purity of 99% (Sigma-Aldrich®, Burlington, MA, USA), methylene blue with purity of 99% (Neon), lead solution 99% (ACS) and commercial activated charcoal from babassu husks (Bahia Carbon).

2.2. Preparation of Biosorbent

Initially, the *Moringa oleifera* Lam. husks were manually peeled and washed with deionized water at 45 °C. Then, the pre-treated seeds were transferred to a 0.1 M nitric acid solution for 1 h and dried in a micro-processed air oven (Digital Timer SX CR/42 Sterilifer, São Caetano do Sul, Brazil) for 12 h. Finally, the material was placed in an oven (Jung 10.012) at 300 °C for 1 h [46]. After cooling, the material was ground and sieved to a size of between 0.35 and 0.50 mm.

2.3. Preparation of Hydrochar

The process involved using agro-industrial residues from *Moringa oleifera* bark using the hydrochar method in which a reactor (WT Accessories) was used.

Moringa oleifera Lam seeds were donated by the Federal University of Sergipe, in Aracaju, Sergipe. Healthy seeds were selected and the husks were manually removed and crushed in an industrial blender (Poli LS04MB, Skymsen, Brusque, Brazil). After separation, the peels were washed with deionized water at a temperature of 60 ± 10 °C to remove coarse impurities present and dried in a microprocessed oven with air circulation (Digital Timer SX CR/42) at 105 °C for 12 h [46,47]. The adsorbent material is called crushed bark (MOH).

After this process, the material was homogenized and the hydrochars were produced in a digital vertical autoclave with a residence time of 6 h at 100 °C and a pressure of 3 bar. The MOH residue was used at a ratio of 1:100 (m/v) [48].

At the end of the period, already at room temperature, the hydrochars were separated from the aqueous phase by filtration, washed with distilled water until a pH close to 6 was reached and dried in an oven for 24 h at 105 °C. After that, the material was separated by granulometry [49].

2.4. Characterization of Adsorbents

After preparing the MOH adsorbent and commercial activated carbon, several techniques were used to characterize the adsorbents in terms of their textural, structural, morphological and chemical composition. The analysis of the zeta potential used a particle analyzer, DelsaTMNanoC (Beckman Coulter, Brea, CA, USA), using the ratio 1:1 (m/v) in the range of pHs from 2 to 12, using solutions of HCl and NaOH 0.1M. Scanning Electron Microscopy (SEM) was analyzed using a Field Emission Scanning Electron Microscope, Quanta 250—FEG (FEI Company, Hillsboro, OR, USA). To carry out the analysis, the samples were coated with gold at a thickness of approximately 30 nm. N_2 physiosorption was performed (BET and BJH models). The samples had previously been dried in an oven for 24 h at 100 °C. Then, the samples were submitted to analysis of adsorption/desorption isotherms recorded at the temperature of liquid nitrogen using the Nova 2000e equipment (Quantachorme, Anton Paar, Graz, Autria). The samples had a pre-treatment at 120 °C for 6 h, in which they were left in a vacuum to remove all moisture and adsorbed species from the surface of the material. Then, they were characterized by N_2 adsorption/desorption isotherms and Fourier transform infrared spectroscopy (FTIR) was used to identify the functional groups present in the studied materials. The Fourier transform infrared spectroscopy technique was conducted using a Vertex 70v spectrophotometer (Bruker, Billerica, MA, USA). To obtain the pellets, they were mixed in KBr at a ratio of 1:1000 (m/m), in the spectral range of 4000 to 400 cm^{-1}.

2.5. Kinetic and Equilibrium Study

Kinetic and equilibrium studies were carried out using batch tests separately for each adsorbent, in which 0.03 g of MOH and commercial activated carbon were used in contact with 30 mL of metformin, diuron, methylene and lead, all with a concentration of 30 mg L^{-1} using HPLC, in which their curves were prepared with the respective pure standards of each solution; each contaminant was standardized at this concentration, so that all were observed at the same concentration, minimizing the adsorption error that would have been possible if the concentrations had been different for each of them. A stirring speed of 150 rpm, pH 7 and a controlled temperature of 25 °C were maintained. The time intervals for withdrawing the aliquots of the analyzed samples were 5, 20, 30, 60, 120, 240, 360, 480, 600, 720, 900, 1080, 1260 and 1440 min, the time required for equilibrium to be reached. The aliquots were filtered through cellulose acetate membranes (0.45 μm) and the final concentrations of contaminants were determined to calculate the adsorption capacity; all tests were performed in duplicate. The percentage of the removal of each contaminant was calculated using Equation (1) as follows:

$$\% \ removal = \frac{C_i - C_f}{C_i} \cdot 100\% \tag{1}$$

where C_i is the initial concentration and C_f is the final concentration, both in mg L^{-1}.

With the final concentration of each sample, the adsorptive capacity (q_e) in mg g^{-1} was calculated as shown in Equation (2):

$$q_e = \frac{\left(C_i - C_f\right)}{m} \cdot V \tag{2}$$

where *V* is the volume of the triclosan solution (L) and m is the mass of the biosorbent (g). To explain the kinetic models, classic models such as pseudo-first-order (PFO) and pseudo-second-order (PSO) were employed.

2.6. Production Cost Analysis

Cost analysis was studied for both adsorbents to report all the expenses involved in the production of the materials, that is, the financial outflows related to production were analyzed. Thus, it was necessary to gather all the details of the expenses relating to the production of the studied materials in order to report the final production cost of each material.

3. Results and Discussion

3.1. Adsorbent Characterizations

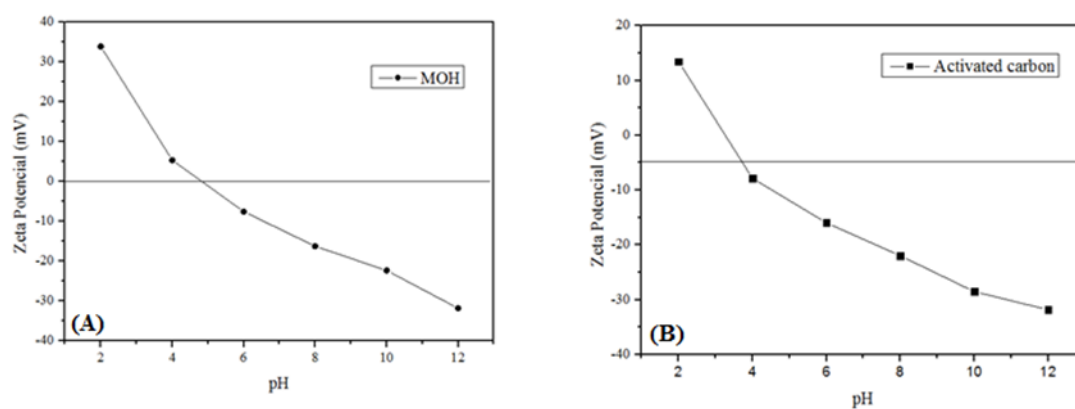Figure 1A,B show the zeta potential of each of the studied adsorbents.

Figure 1. Zeta potential of (**A**) MOH and (**B**) activated carbon.

Note that Figure 1A,B show the values obtained for the zeta potential of both adsorbents at different pHs (2–12) [46]. It is observed that in Figure 1A, the isoelectric point occurred close to pH 5.5, demonstrating that at a pH greater than 5.5 its charge is negative and at a lower pH its charge is positive [47]. As for Figure 1B, the isoelectric point was at pH 4; therefore, a pH lower than 4 has a positive charge and a pH greater than 4 has a negative charge. And in both cases it is observed that the zeta potential was negative [48]. This means that the points used show an interaction between the studied contaminants and their studied adsorbents.

Both samples underwent SEM analysis, in order to evaluate the morphology of the studied materials, as shown in Figure 2A,B.
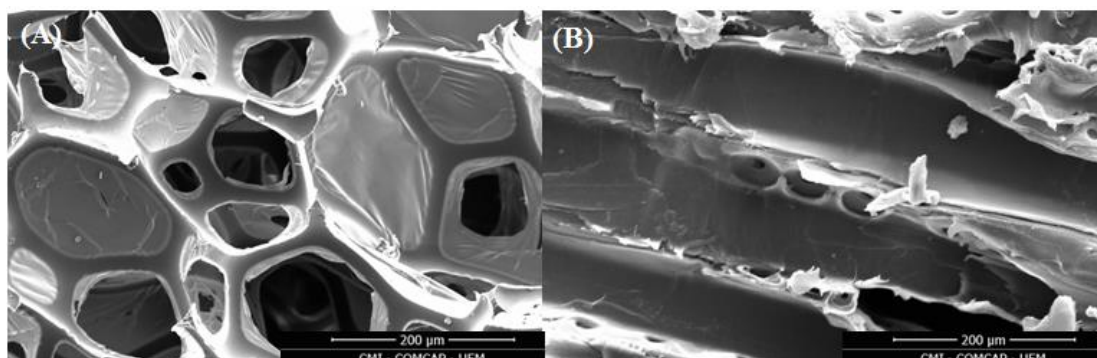

Figure 2. SEM of (**A**) MOH and (**B**) activated carbon.

It is observed that in Figure 2A, with 2000× magnitude, the MOH material has cavities with defined and heterogeneous pores, favoring the adsorption of contaminants

and confirming that the process used to produce the material is favorable for the adsorption process; and in Figure 2B, with 2000× magnitude, there is a large number of pore cavities and also heterogeneous pores that greatly facilitate the adsorption of contaminants and allow greater use of the material [49,50].

A BET analysis of both materials was carried out in order to evaluate their porosity. Because this specific area contributes to the adsorption of contaminants, Table 1 shows the values obtained.

Table 1. BET analysis of the MOH and activated carbon.

	MOH	Activated Carbon
BET specific surface area ($m^2 \, g^{-1}$)	38.25	205.71
Average pore diameter (Å)	26.44	32.57
Total pore volume ($cm^3 \, g^{-1}$)	0.1293	0.4899
Micropore volume ($cm^3 \, g^{-1}$)	0.0996	0.4012
Mesopore volume ($cm^3 \, g^{-1}$)	0.0297	0.0887

Based on Table 1, the adsorbents studied have a relatively high area for the adsorption process. According to IUPAC, porous materials can be classified as macropores, mesopores and micropores. It is observed that both materials had a predominance of micropores; this fact is important for the removal of contaminants that are often difficult to remove [51,52].

To determine the functional groups of the materials, FTIR analysis was performed for the two adsorbents studied, as shown in Figure 3A,B.
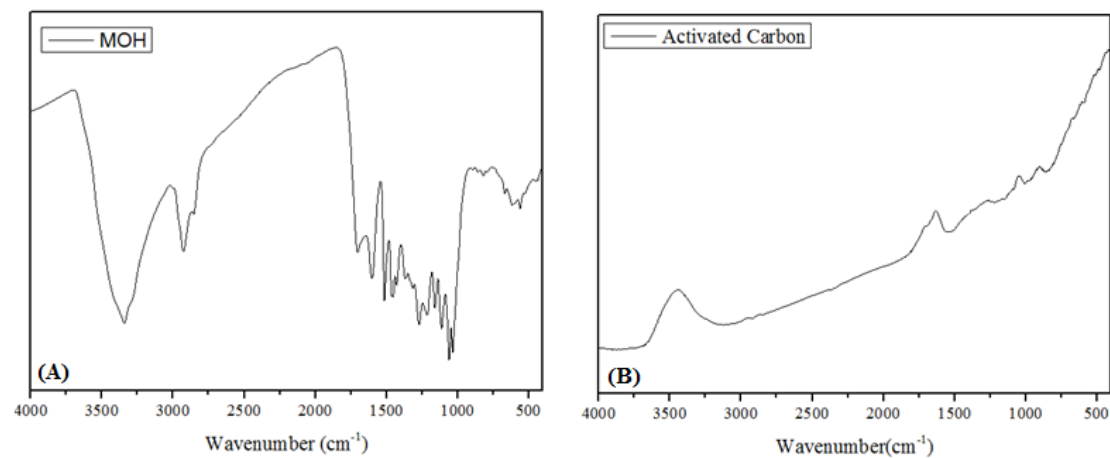

Figure 3. FTIR for (**A**) MOH and (**B**) activated carbon.

Note that in Figure 3A the MOH adsorbent material has a large and wide band of 3421–3329 cm^{-1}, possibly indicating hydrogen bonding, a characteristic of organic material [53]. The presence of the peak for the region of 2921 cm^{-1} demonstrates and determines the presence of methylcellulose, due to the possibility of asymmetric stretching of the C-H bond present in the CH_2 group [54]. Note that in the performed spectrum it has a peak of 2809 cm^{-1}, which refers to a symmetrical stretching of the C-H bond of the CH_3 group. In the region, the value of 1569 cm^{-1} is observed, with an increase in this relative area and with the modification of the peak to the region of 1521 cm^{-1} [55]. This change is possibly related to the stretching of the COO-bonds and also partly to the N-H deformation of the amine groups, which may be secondary [56]. The peak region at 1072 cm^{-1} is characterized by the C-O region, which includes the possible structures of lignin, cellulose and hemicellulose, which make up all the analyzed material [57]. As for the FTIR of the activated carbon (Figure 3B), an increase in intensity between 3540 and 3351 cm^{-1} is observed, characterizing a typical (OH) absorption band, which is normally also associated with the presence of hydrogen [58]. This absorption can be attributed to the predominant presence of the OH

groups of phenols, since, in general, the significant presence of the (OH) of carboxylic groups in AC is characterized by strong absorption, which extends up to 2892 cm^{-1} [59]. The increase in intensity between 1681 and 1593 cm^{-1} evidences the presence of C=O carbonyl groups that exist in carboxylic acids, ketones and in cellulose itself [60]. The presence of the band at approximately 1477 cm^{-1} can be attributed to vibrations of typical aromatic rings in carbonaceous materials. The peak between 1068 and 1004 cm^{-1} can be attributed to the stretching of the C-O bond corresponding to the vibrations of the phenolic groups [61]. A lower intensity peak close to 673 cm^{-1} confirms the presence of ether and lactone [62].

3.2. Kinetic and Equilibrium Study

The use of the natural pH of each sample was chosen so that there would not be any kind of modification of the physical–chemical characteristics, which could alter the results. The importance of kinetic and equilibrium studies for the adsorption process is essential to understand the adsorption behavior of contaminants in relation to time, because in this study the removal of the contaminant is reported in relation to the adsorbent studied, as shown in Figures 4 and 5.
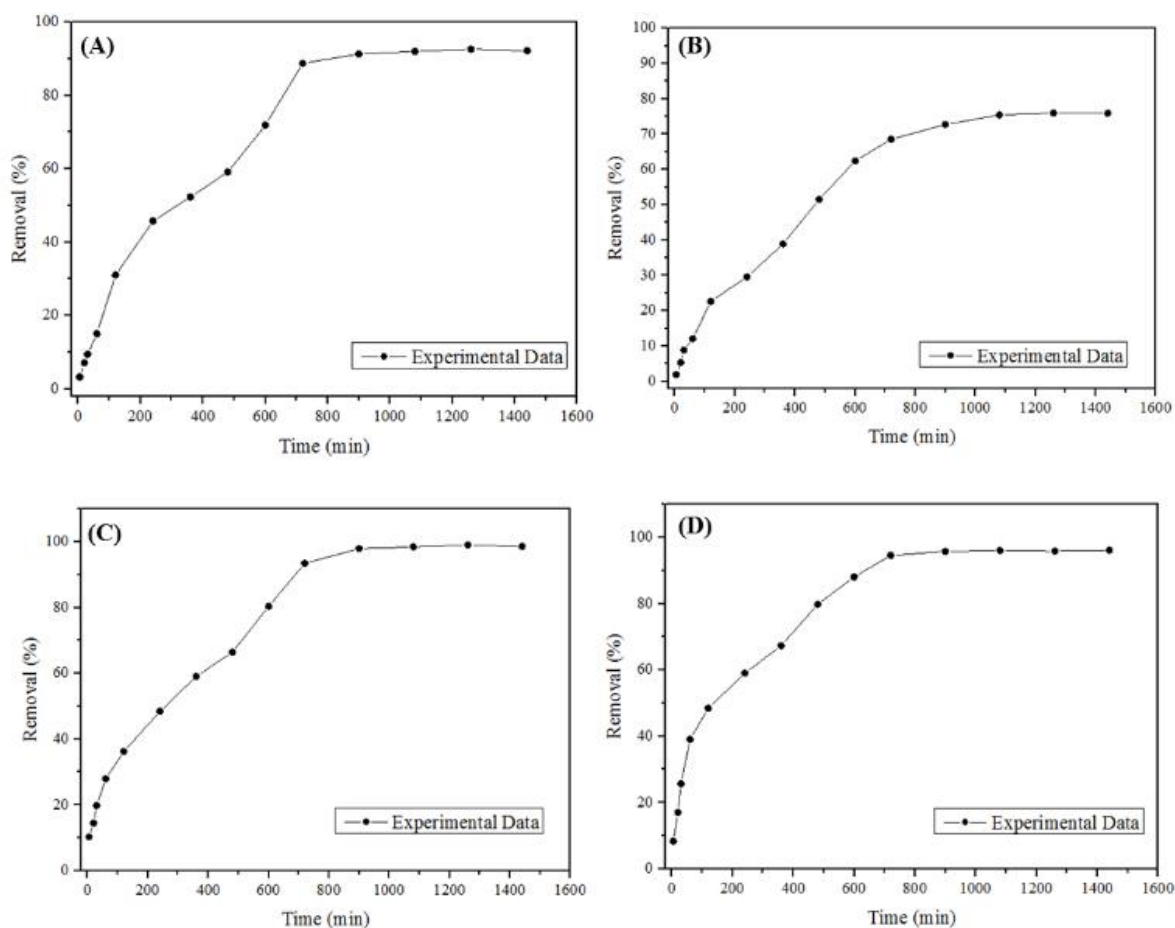

Figure 4. Removal and adsorption equilibrium of the contaminants studied with MOH: (**A**) metformin, (**B**) diuron, (**C**) methylene blue, (**D**) lead.
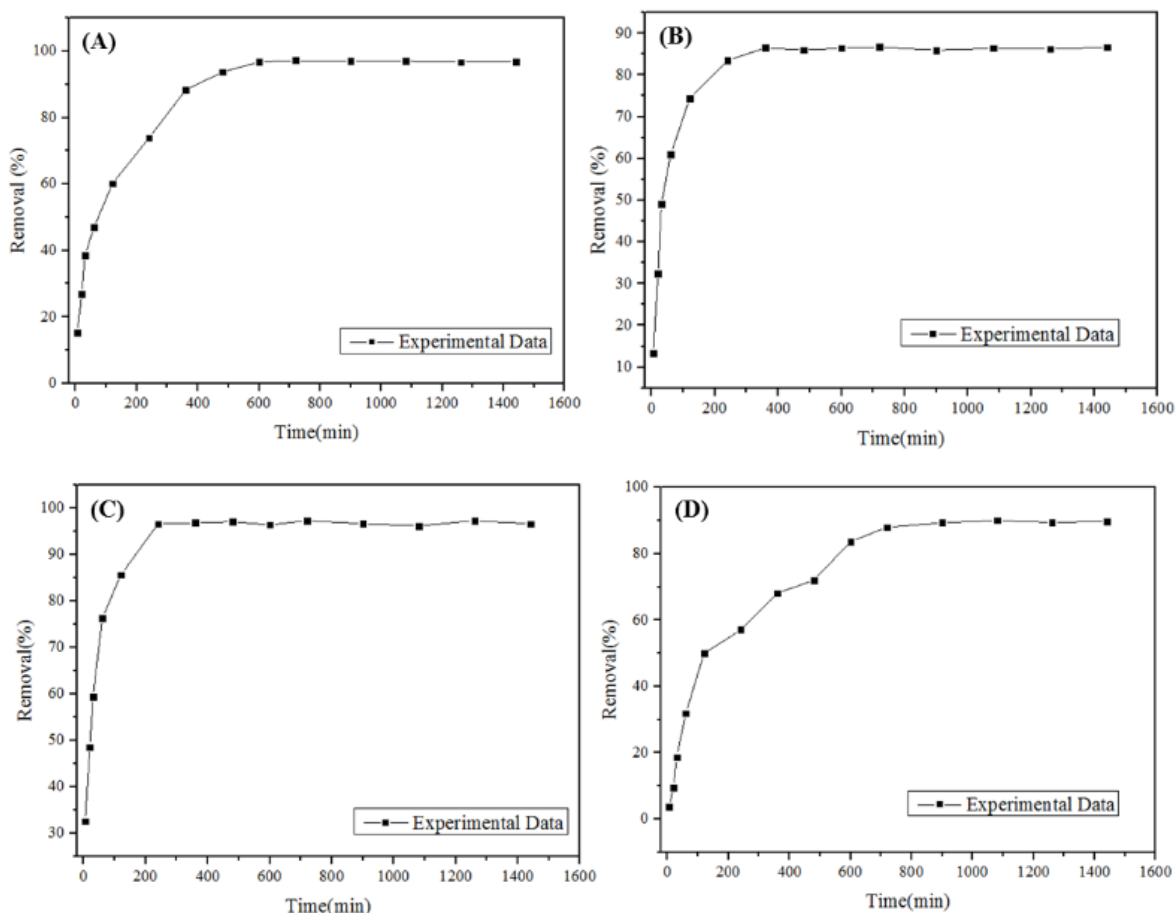
Figure 5. Removal and adsorption equilibrium of the contaminants studied with activated carbon: (**A**) metformin, (**B**) diuron, (**C**) methylene blue, (**D**) lead.

In Figure 4, we show the kinetic studies and chemical balance of the four contaminants used for the MOH, using the natural pH of each sample. The zeta potential reported that the isoelectric charge was 5.5. In Figure 4A, the removal of the metformin is visualized. It is observed that, in the initial moments of removal, significant removal occurred, possibly demonstrating that there is a good interaction of the active sites with the metformin. As the removal time passes, a slower removal is observed, since the active sites were probably already saturated. Stability occurred in approximately 900 min, as, from that point on, the equilibrium state of the reaction was characterized; that is, the active sites were fully saturated and thus there was no interaction with the metformin, making it impossible for new molecules to enter the cavities of the active site. The percentage of the removal was 93.54% with $q_e = 28.05$ mg g^{-1}. In Figure 4B, the removal of the contaminant diuron is shown. It is observed that the contaminant also had a good interaction with the MOH. In the initial moments, the removal occurred more slowly and, with the passage of time, there was an interaction of the adsorbent with the contaminant. This fact can be explained because diuron molecules are larger and possibly quickly saturated the cavities of the active sites. Equilibrium occurred in 1200 min with a removal percentage of 84.56% with $q_e = 25.36$ mg g^{-1}. Figure 4C shows the removal of the methylene blue dye, which had the greatest interaction with the MOH. In the initial phase, there was a very expressive removal, proving that the contaminant molecules quickly occupied the active sites of the material. Over time, this interaction increased, reaching the equilibrium point at approximately 800 min and with a maximum removal of 99.13% with $q_e = 29.74$ mg g^{-1}. And in Figure 4D, relating to the heavy metal lead, this contaminant had a high interaction with the studied material. At the beginning of the removal process, it took place at a slower pace, since the

difficulty of removing the contaminant is high. Over time, this interaction increased and allowed the removal to take place, where it was verified that balance occurred in 700 min and with a removal of 93.45% with q_e = 28.04 mg g^{-1}, proving that there was interaction with the adsorbent. Briefly, the MOH, for the four contaminants studied, obtained a good relationship and good removals. The PFO and PSO models for the MOH were determined and are presented in Table 2.

Table 2. Kinetic models for biosorption by MOH.

Models	Parameters	Metformin	Diuron	Methylene Blue	Lead
PFO	q_e (mg g^{-1})	29.65	27.13	31.07	30.20
	k_1 (min^{-1})	0.008	0.013	0.009	0.015
	R^2	0.962	0.9703	0.991	0.957
	χ^2	0.189	0.234	0.218	0.245
PSO	q_e (mg g^{-1})	25.17	21.22	30.78	27.45
	k_2 (g mg^{-1} min^{-1})	0.012	0.023	0.011	0.033
	R^2	0.907	0.921	0.934	0.893
	χ^2	0.267	0.328	0.437	0.578

Figure 5 demonstrates the removal of the same contaminants seen in Figure 4, but with another adsorbent material, which in this case was activated carbon.

In Figure 5A, the removal of the metformin contaminant by the activated carbon is observed. In this case, it is related to the high interaction of the material using the natural pH of each sample. The zeta potential shows that the isoelectric charge was 4.0, and this fact can also be explained with reference to Table 1. With the high number of cavities in this studied material, the large number of pores quickly sequestered the metformin. It is observed that balance occurred in approximately 600 min and with a removal of 97.05% with q_e = 29.5 mg g^{-1}, proving that there is a high interaction between the adsorbent and adsorbate. In Figure 5B, the activated carbon was used to remove the pesticide diuron, which had a good interaction in the initial phase with high removal rates, as its molecules are extensive and easy to remove initially. Over time, the diuron had its removal decreased from its aqueous solution, and stability occurred in approximately in 500 min. Without it having further significant variation in the removal percentage, it can be stated that there was a state of equilibrium: the empty active sites were decreasing, which made it difficult to adsorb the diuron molecules. After stability was achieved in the kinetic study, the maximum removal percentage was 86.53% with q_e = 25.90 mg g^{-1}.

Figure 5C reports the use of the activated carbon to remove the methylene blue dye, which is widely used in Brazil in textile industries for dyeing clothes, which consequently generates a significant amount of effluent. It is observed that there are high rates of removals in the initial phase, as there is an excellent interaction of the material with the aqueous solution of the methylene blue, because the adsorbate molecule is considered a macromolecule and with that high removals happen with the passage of time. With time, the removal speed decreases because the cavities of the active sites become saturated, making it difficult for new molecules to enter the adsorbent. The equilibrium study shows that equilibrium occurred in approximately 300 min, that is, after that moment there was no more interaction between the adsorbent and adsorbate; the removal reached the value of 98.76% with q_e = 29.61 mg g^{-1}. In Figure 5D, the removal of the lead using the activated carbon is shown. It is noted that in the initial moments there is also an interaction between the adsorbent and adsorbate. With the passage of time, the adsorptive process decreases, since the pores are saturated with the lead molecules, making it difficult to remove the contaminant. Equilibrium occurs in approximately 900 min with no further interaction between the adsorbent and adsorbate; the maximum removal of the contaminant was 87.45% with q_e = 26.4 mg g^{-1}. In general, activated carbon is a good adsorbent for

removing the four contaminants studied compared to MOH. The PFO and PSO models for the active carbon were determined and are presented in Table 3.

Table 3. Kinetic models for biosorption by active carbon.

Models	Parameters	Metformin	Diuron	Methylene Blue	Lead
PFO	q_e (mg g^{-1})	32.34	27.76	32.10	27.86
	k_1 (min^{-1})	0.004	0.009	0.005	0.008
	R^2	0.973	0.981	0.994	0.975
	χ^2	0.109	0.156	0.153	0.147
PSO	q_e (mg g^{-1})	30.72	24.55	28.83	23.67
	k_2 (g mg^{-1} min^{-1})	0.009	0.013	0.009	0.025
	R^2	0.942	0.954	0.962	0.913
	χ^2	0.203	0.293	0.374	0.278

3.3. Study Production Cost of Each Adsorbent

In Table 4, the production costs of each material used in this study are shown. The costs are in the local currency of Brazil (BRL) and are presented below.

Table 4. Production costs of each material.

Activated Carbon	
Production	**Cost (BRL/kg)**
Activated carbon (commercial)	35.00
Total cost	35.00
MOH	
Production	**Cost (BRL/kg)**
Raw material (waste)	0.00
Water wash	1.25
Material drying	1.05
Crushing of the material	2.00
Hydrothermal reactor processing	3.25
Material drying	1.05
Granulometry separation	0.80
Total cost	9.4

It is observed that the commercial activated carbon has a final production price in kg of BRL 35.00. The process is more expensive when compared to that required for the MOH, because in the process the activation of the material is carried out, requiring a large amount of reagent to carry out the process. But on the other hand, the material has a high surface area, as seen in Table 1. In comparison, the MOH is a material developed from agro-industrial waste through the hydrochar process, in which only water and pressure are used in a given time [63]. The production cost in kg was BRL 9.4, approximately 3.72 times lower than that of the activated carbon. As seen in Table 1, the material does not have a high specific area compared to the activated carbon. However, its micropore volumes are high and, therefore, the studied material has a good interaction with many contaminants, which, consequently, can be removed. In turn, the MOH material was determined to have low-cost production, profitability, easy production and interactions with contaminants that need to be removed from the environment [64].

4. Conclusions

This study evaluated the production of an adsorbent from agro-industrial waste and compared it with a commercial adsorbent, activated carbon. The MOH characterization demonstrated that the material was a good alternative for large-scale production in the

future. The study was carried out to remove emerging contaminants, namely, metformin, diuron, methylene blue and lead, and showed removal rates ranging from 84.56 to 99.13%. And in relation to the cost of producing the material, this was another important point to evaluate, since the residue is completely discarded without commercial purposes and the hydrochar production process is much cheaper than that for activated carbon, around 3.72 times lower. In addition, with high values of the total volume of mesopores, the material becomes efficient, low-cost and easy to obtain, presenting a good potential as an adsorbent and being suitable for use on a commercial scale in the future for water and wastewater treatment.

References

1. Naidoo, T.; Rajkaran, A. Sershen Impacts of Plastic Debris on Biota and Implications for Human Health: A South African Perspective. *S. Afr. J. Sci.* **2020**, *116*, 1–8. [CrossRef] [PubMed]
2. Shakibaie, M.; Mohazab, N.S.; Ayatollahi Mousavi, S.A. Antifungal Activity of Selenium Nanoparticles Synthesized by Bacillus Species Msh-1 against Aspergillus Fumigatus and Candida Albicans. *Jundishapur J. Microbiol.* **2015**, *8*, e26381. [CrossRef] [PubMed]
3. Crini, G.; Badot, P.M. Application of Chitosan, a Natural Aminopolysaccharide, for Dye Removal from Aqueous Solutions by Adsorption Processes Using Batch Studies: A Review of Recent Literature. *Prog. Polym. Sci.* **2008**, *33*, 399–447. [CrossRef]
4. Gülçek, B.; Tepe, O. Removal of Atrazine by Biogenic Manganese Oxide in Batch and Fixed-Bed Column Reactors. *Geomicrobiol. J.* **2022**, *39*, 17–27. [CrossRef]
5. Quesada, H.B.; Baptista, A.T.A.; Cusioli, L.F.; Seibert, D.; Bezerra, C.d.O.; Bergamasco, R. Surface Water Pollution by Pharmaceuticals and an Alternative of Removal by Low-Cost Adsorbents: A Review. *Chemosphere* **2019**, *222*, 766–780. [CrossRef] [PubMed]
6. Cusioli, L.F.; Quesada, H.B.; Barbosa de Andrade, M.; Gomes, R.G.; Bergamasco, R. Application of a Novel Low-Cost Adsorbent Functioned with Iron Oxide Nanoparticles for the Removal of Triclosan Present in Contaminated Water. *Microporous Mesoporous Mater.* **2021**, *325*, 111328. [CrossRef]
7. Luo, Y.; Guo, W.; Ngo, H.H.; Nghiem, L.D.; Hai, F.I.; Zhang, J.; Liang, S.; Wang, X.C. A Review on the Occurrence of Micropollutants in the Aquatic Environment and Their Fate and Removal during Wastewater Treatment. *Sci. Total Environ.* **2014**, *473–474*, 619–641. [CrossRef]
8. Gahlawat, G.; Choudhury, A.R. A Review on the Biosynthesis of Metal and Metal Salt Nanoparticles by Microbes. *RSC Adv.* **2019**, *9*, 12944–12967. [CrossRef]
9. Bezerra, C.d.O.; Cusioli, L.F.; Quesada, H.B.; Nishi, L.; Mantovani, D.; Vieira, M.F.; Bergamasco, R. Assessment of the Use of *Moringa oleifera* Seed Husks for Removal of Pesticide Diuron from Contaminated Water. *Environ. Technol.* **2018**, *41*, 191–201. [CrossRef]
10. Grundgeiger, E.; Lim, Y.H.; Frost, R.L.; Ayoko, G.A.; Xi, Y. Application of Organo-Beidellites for the Adsorption of Atrazine. *Appl. Clay Sci.* **2015**, *105–106*, 252–258. [CrossRef]
11. Al-Shaalan, N.H.; Ali, I.; ALOthman, Z.A.; Al-Wahaibi, L.H.; Alabdulmonem, H. High Performance Removal and Simulation Studies of Diuron Pesticide in Water on MWCNTs. *J. Mol. Liq.* **2019**, *289*, 111039. [CrossRef]
12. Chen, H.; Luo, Y.; Potter, C.; Moran, P.J.; Grieneisen, M.L.; Zhang, M. Modeling Pesticide Diuron Loading from the San Joaquin Watershed into the Sacramento-San Joaquin Delta Using SWAT. *Water Res.* **2017**, *121*, 374–385. [CrossRef]
13. Bhoi, Y.P.; Behera, C.; Majhi, D.; Equeenuddin, S.M.; Mishra, B.G. Visible Light-Assisted Photocatalytic Mineralization of Diuron Pesticide Using Novel Type II CuS/Bi2W2O9 Heterojunctions with a Hierarchical Microspherical Structure. *New J. Chem.* **2018**, *42*, 281–292. [CrossRef]
14. Silambarasan, S.; Cornejo, P.; Vangnai, A.S. Biodegradation of 4-Nitroaniline by Novel Isolate Bacillus Sp. Strain AVPP64 in the Presence of Pesticides. *Environ. Pollut.* **2022**, *306*, 119453. [CrossRef]

15. Velki, M.; Lackmann, C.; Barranco, A.; Ereño Artabe, A.; Rainieri, S.; Hollert, H.; Seiler, T.B. Pesticides Diazinon and Diuron Increase Glutathione Levels and Affect Multixenobiotic Resistance Activity and Biomarker Responses in Zebrafish (Danio Rerio) Embryos and Larvae. *Environ. Sci. Eur.* **2019**, *31*, 4. [CrossRef]

16. Metcalfe, C.D.; Miao, X.S.; Koenig, B.G.; Struger, J. Distribution of Acidic and Neutral Drugs in Surface Waters near Sewage Treatment Plants in the Lower Great Lakes, Canada. *Environ. Toxicol. Chem.* **2003**, *22*, 2881–2889. [CrossRef]

17. Daughton, C.G. Cradle-to-Cradle Stewardship of Drugs for Minimizing Their Environmental Disposition While Promoting Human Health. I. Rational for and Avenues toward a Green Pharmacy. *Environ. Health Perspect.* **2003**, *111*, 757–774. [CrossRef]

18. Carmona, E.; Andreu, V.; Picó, Y. Multi-Residue Determination of 47 Organic Compounds in Water, Soil, Sediment and Fish—Turia River as Case Study. *J. Pharm. Biomed. Anal.* **2017**, *146*, 117–125. [CrossRef]

19. Jakubiec-Krzesniak, K.; Rajnisz-Mateusiak, A.; Guspiel, A.; Ziemska, J.; Solecka, J. Secondary Metabolites of Actinomycetes and Their Antibacterial, Antifungal and Antiviral Properties. *Pol. J. Microbiol.* **2018**, *67*, 259–272. [CrossRef]

20. Scheurer, M.; Michel, A.; Brauch, H.J.; Ruck, W.; Sacher, F. Occurrence and Fate of the Antidiabetic Drug Metformin and Its Metabolite Guanylurea in the Environment and during Drinking Water Treatment. *Water Res.* **2012**, *46*, 4790–4802. [CrossRef]

21. Oladoye, P.O.; Ajiboye, T.O.; Omotola, E.O.; Oyewola, O.J. Methylene Blue Dye: Toxicity and Potential Elimination Technology from Wastewater. *Results Eng.* **2022**, *16*, 100678. [CrossRef]

22. Katre, U.V.; Suresh, C.G.; Khan, M.I.; Gaikwad, S.M. Structure–Activity Relationship of a Hemagglutinin from *Moringa oleifera* Seeds. *Int. J. Biol. Macromol.* **2008**, *42*, 203–207. [CrossRef] [PubMed]

23. Ostaszewski, P.; Długosz, O.; Banach, M. Analysis of Measuring Methods of the Concentration of Methylene Blue in the Sorption Process in Fixed-Bed Column. *Int. J. Environ. Sci. Technol.* **2022**, *19*, 1–8. [CrossRef]

24. Zein, R.; Satrio Purnomo, J.; Ramadhani, P.; Safni; Alif, M.F.; Putri, C.N. Enhancing Sorption Capacity of Methylene Blue Dye Using Solid Waste of Lemongrass Biosorbent by Modification Method. *Arab. J. Chem.* **2023**, *16*, 104480. [CrossRef]

25. Saeed, A.A.H.; Harun, N.Y.; Sufian, S.; Siyal, A.A.; Zulfiqar, M.; Bilad, M.R.; Vagananthan, A.; Al-Fakih, A.; Ghaleb, A.A.S.; Almahbashi, N. Eucheuma Cottonii Seaweed-Based Biochar for Adsorption of Methylene Blue Dye. *Sustainability* **2020**, *12*, 10318. [CrossRef]

26. Soria-Aguilar, M.d.J.; Martínez-Luévanos, A.; Sánchez-Castillo, M.A.; Carrillo-Pedroza, F.R.; Toro, N.; Narváez-García, V.M. Removal of Pb(II) from Aqueous Solutions by Using Steelmaking Industry Wastes: Effect of Blast Furnace Dust's Chemical Composition. *Arab. J. Chem.* **2021**, *14*, 103061. [CrossRef]

27. Khedr, R.F. Synthesis of Amidoxime Adsorbent by Radiation-Induced Grafting of Acrylonitrile/Acrylic Acid on Polyethylene Film and Its Application in Pb Removal. *Polymers* **2022**, *14*, 3136. [CrossRef]

28. Tangahu, B.V.; Sheikh Abdullah, S.R.; Basri, H.; Idris, M.; Anuar, N.; Mukhlisin, M. Lead (Pb) Removal from Contaminated Water Using Constructed Wetland Planted with Scirpus Grossus: Optimization Using Response Surface Methodology (RSM) and Assessment of Rhizobacterial Addition. *Chemosphere* **2022**, *291*, 132952. [CrossRef]

29. Ramola, S.; Rawat, N.; Shankhwar, A.K.; Srivastava, R.K. Fixed Bed Adsorption of Pb and Cu by Iron Modified Bamboo, Bagasse and Tyre Biochar. *Sustain. Chem. Pharm.* **2021**, *22*, 100486. [CrossRef]

30. Narayana, P.L.; Lingamdinne, L.P.; Karri, R.R.; Devanesan, S.; AlSalhi, M.S.; Reddy, N.S.; Chang, Y.Y.; Koduru, J.R. Predictive Capability Evaluation and Optimization of Pb(II) Removal by Reduced Graphene Oxide-Based Inverse Spinel Nickel Ferrite Nanocomposite. *Environ. Res.* **2022**, *204*, 112029. [CrossRef]

31. de Souza, R.M.; Seibert, D.; Quesada, H.B.; de Jesus Bassetti, F.; Fagundes-Klen, M.R.; Bergamasco, R. Occurrence, Impacts and General Aspects of Pesticides in Surface Water: A Review. *Process Saf. Environ. Prot.* **2020**, *135*, 22–37. [CrossRef]

32. Alizadeh Fard, M.; Barkdoll, B. Magnetic Activated Carbon as a Sustainable Solution for Removal of Micropollutants from Water. *Int. J. Environ. Sci. Technol.* **2019**, *16*, 1625–1636. [CrossRef]

33. Eniola, J.O.; Kumar, R.; Barakat, M.A.; Rashid, J. A Review on Conventional and Advanced Hybrid Technologies for Pharmaceutical Wastewater Treatment. *J. Clean. Prod.* **2022**, *356*, 131826. [CrossRef]

34. Metz, F.; Glaus, A. Integrated Water Resources Management and Policy Integration: Lessons from 169 Years of Flood Policies in Switzerland. *Water* **2019**, *11*, 1173. [CrossRef]

35. Reck, I.M.; Paixão, R.M.; Bergamasco, R.; Vieira, M.F.; Vieira, A.M.S. Removal of Tartrazine from Aqueous Solutions Using Adsorbents Based on Activated Carbon and *Moringa oleifera* Seeds. *J. Clean. Prod.* **2018**, *171*, 85–97. [CrossRef]

36. Baptista, A.T.A.; Coldebella, P.F.; Cardines, P.H.F.; Gomes, R.G.; Vieira, M.F.; Bergamasco, R.; Vieira, A.M.S. Coagulation-Flocculation Process with Ultrafiltered Saline Extract of *Moringa oleifera* for the Treatment of Surface Water. *Chem. Eng. J.* **2015**, *276*, 166–173. [CrossRef]

37. Ueda Yamaguchi, N.; Cusioli, L.F.; Quesada, H.B.; Camargo Ferreira, M.E.; Fagundes-Klen, M.R.; Salcedo Vieira, A.M.; Gomes, R.G.; Vieira, M.F.; Bergamasco, R. A Review of *Moringa oleifera* Seeds in Water Treatment: Trends and Future Challenges. *Process Saf. Environ. Prot.* **2021**, *147*, 405–420. [CrossRef]

38. Beluci, N.d.C.L.; Mateus, G.A.P.; Miyashiro, C.S.; Homem, N.C.; Gomes, R.G.; Fagundes-Klen, M.R.; Bergamasco, R.; Vieira, A.M.S. Hybrid Treatment of Coagulation/Flocculation Process Followed by Ultrafiltration in TiO_2-Modified Membranes to Improve the Removal of Reactive Black 5 Dye. *Sci. Total Environ.* **2019**, *664*, 222–229. [CrossRef]

39. Suarez, M.; Haenni, M.; Canarelli, S.; Fisch, F.; Chodanowski, P.; Servis, C.; Michielin, O.; Freitag, R.; Moreillon, P.; Mermod, N. Structure-Function Characterization and Optimization of a Plant-Derived Antibacterial Peptide. *Antimicrob. Agents Chemother.* **2005**, *49*, 3847–3857. [CrossRef]

40. Cusioli, L.F.; Mantovani, D.; Quesada, H.B.; Gomes, R.G.; Bergamasco, R. Adsorption of COVID-19-Related Drug from Contaminated Water Using Activated Carbon. *Desalination Water Treat.* **2022**, *277*, 85–89. [CrossRef]

41. Cusioli, L.F.; Bezerra, C.d.O.; Quesada, H.B.; Alves Baptista, A.T.; Nishi, L.; Vieira, M.F.; Bergamasco, R. Modified *Moringa oleifera* Lam. Seed Husks as Low-Cost Biosorbent for Atrazine Removal. *Environ. Technol.* **2019**, *42*, 1092–1103. [CrossRef]

42. Wernke, G.; Fagundes-Klen, M.R.; Vieira, M.F.; Suzaki, P.Y.R.; de Souza, H.K.S.; Shimabuku, Q.L.; Bergamasco, R. Mathematical Modelling Applied to the Rate-Limiting Mass Transfer Step Determination of a Herbicide Biosorption onto Fixed-Bed Columns. *Environ. Technol.* **2018**, *41*, 638–648. [CrossRef] [PubMed]

43. Leng, L.; Yang, L.; Leng, S.; Zhang, W.; Zhou, Y.; Peng, H.; Li, H.; Hu, Y.; Jiang, S.; Li, H. A Review on Nitrogen Transformation in Hydrochar during Hydrothermal Carbonization of Biomass Containing Nitrogen. *Sci. Total Environ.* **2021**, *756*, 143679. [CrossRef]

44. Wang, T.; Zhai, Y.; Zhu, Y.; Li, C.; Zeng, G. A Review of the Hydrothermal Carbonization of Biomass Waste for Hydrochar Formation: Process Conditions, Fundamentals, and Physicochemical Properties. *Renew. Sustain. Energy Rev.* **2018**, *90*, 223–247. [CrossRef]

45. Liu, H.; Basar, I.A.; Nzihou, A.; Eskicioglu, C. Hydrochar Derived from Municipal Sludge through Hydrothermal Processing: A Critical Review on Its Formation, Characterization, and Valorization. *Water Res.* **2021**, *199*, 117186. [CrossRef]

46. Regalbuto, J.R.; Robles, J.O. *The Engineering of Pt/Carbon Catalyst Preparation*; University of Illinois: Chicago, IL, USA, 2004; Volume 1, pp. 1–14.

47. Bhattacharjee, S. DLS and Zeta Potential—What They Are and What They Are Not? *J. Control. Release* **2016**, *235*, 337–351. [CrossRef] [PubMed]

48. Chibowski, E.; Szcześ, A. Zeta Potential and Surface Charge of DPPC and DOPC Liposomes in the Presence of PLC Enzyme. *Adsorption* **2016**, *22*, 755–765. [CrossRef]

49. Kiwumulo, H.F.; Muwonge, H.; Ibingira, C.; Lubwama, M.; Kirabira, J.B.; Ssekitoleko, R.T. Green Synthesis and Characterization of Iron-Oxide Nanoparticles Using *Moringa oleifera*: A Potential Protocol for Use in Low and Middle Income Countries. *BMC Res. Notes* **2022**, *15*, 149. [CrossRef]

50. Wibawa, P.J.; Nur, M.; Asy'ari, M.; Nur, H. SEM, XRD and FTIR Analyses of Both Ultrasonic and Heat Generated Activated Carbon Black Microstructures. *Heliyon* **2020**, *6*, e03546. [CrossRef]

51. Adebayo, G.B.; Jamiu, W.; Okoro, H.K.; Okeola, F.O.; Adesina, A.K.; Feyisetan, O.A. Kinetics, Thermodynamics and Isothermal Modelling of Liquid Phase Adsorption of Methylene Blue onto Moringa Pod Husk Activated Carbon. *S. Afr. J. Chem.* **2019**, *72*, 263–273. [CrossRef]

52. Saka, C. BET, TG-DTG, FT-IR, SEM, Iodine Number Analysis and Preparation of Activated Carbon from Acorn Shell by Chemical Activation with $ZnCl_2$. *J. Anal. Appl. Pyrolysis* **2012**, *95*, 21–24. [CrossRef]

53. Cruz-Espinoza, J.E.; Orduña-Díaz, A.; Rosales-Perez, M.; Zaca-Morán, O.; Delgado-Macuil, R.; Gayou, V.L.; Rojas-López, M. FTIR Analysis of Phenolic Extracts from *Moringa oleifera* Leaves. *J. Biom. Biostat.* **2012**, *11*, 2802.

54. Hashim, F.J.; Mathkor, T.H.; Hussein, H.; Shawkat, M.S. GC-MS and FTIR Analysis of *Moringa oleifera* Leaves Different Extracts and Evaluation of Their Antioxidant Activity. *Asian J. Microbiol. Biotechnol. Environ. Sci.* **2017**, *19*, 861–871.

55. Coldebella, P.F.; Fagundes-klen, R.; Valverde, K.C.; Cavalcanti, E.B.; Aparecida, O. Potential Effect of Chemical and Thermal Treatment on the Kinetics, Equilibrium, and Thermodynamic Studies for Atrazine Biosorption by the *Moringa oleifera* Pods. *Can. J. Chem. Eng.* **2017**, *95*, 961–973. [CrossRef]

56. Sya'banah, N.; Yulianti, E.; Istighfarini, V.N.; Lutfia, F.N.L. Characterization and Effectiveness of *Moringa oleifera* Seeds Extract as a Phosphate Coagulant. *J. Neutrino* **2020**, *12*, 57–64. [CrossRef]

57. Dalhoumi, W.; Guesmi, F.; Bouzidi, A.; Akermi, S.; Hfaiedh, N.; Saidi, I. Therapeutic Strategies of *Moringa oleifera* Lam. (Moringaceae) for Stomach and Forestomach Ulceration Induced by HCl/EtOH in Rat Model. *Saudi J. Biol. Sci.* **2022**, *29*, 103284. [CrossRef]

58. Joga Rao, H. Characterization Studies on Adsorption of Lead and Cadmium Using Activated Carbon Prepared from Waste Tyres. *Nat. Environ. Pollut. Technol.* **2021**, *20*, 561–568. [CrossRef]

59. Dittmann, D.; Saal, L.; Zietzschmann, F.; Mai, M.; Altmann, K.; Al-Sabbagh, D.; Schumann, P.; Ruhl, A.S.; Jekel, M.; Braun, U. Characterization of Activated Carbons for Water Treatment Using TGA-FTIR for Analysis of Oxygen-Containing Functional Groups. *Appl. Water Sci.* **2022**, *12*, 203. [CrossRef]

60. González-González, R.B.; González, L.T.; Madou, M.; Leyva-Porras, C.; Martinez-Chapa, S.O.; Mendoza, A. Synthesis, Purification, and Characterization of Carbon Dots from Non-Activated and Activated Pyrolytic Carbon Black. *Nanomaterials* **2022**, *12*, 298. [CrossRef]

61. Hussain, O.A.; Hathout, A.S.; Abdel-Mobdy, Y.E.; Rashed, M.M.; Abdel Rahim, E.A.; Fouzy, A.S.M. Preparation and Characterization of Activated Carbon from Agricultural Wastes and Their Ability to Remove Chlorpyrifos from Water. *Toxicol. Rep.* **2023**, *10*, 146–154. [CrossRef]

62. Mistar, E.M.; Alfatah, T.; Supardan, M.D. Synthesis and Characterization of Activated Carbon from Bambusa Vulgaris Striata Using Two-Step KOH Activation. *J. Mater. Res. Technol.* **2020**, *9*, 6278–6286. [CrossRef]

63. Osborne, S.P.; Nasi, G.; Powell, M. Beyond Co-Production: Value Creation and Public Services. *Public Adm.* **2021**, *99*, 641–657. [CrossRef]

64. Bahşi, N.; Çetin, E. Determining of Agricultural Credit Impact on Agricultural Production Value in Turkey. *Cienc. Rural* **2020**, *50*, e20200003. [CrossRef]